

1       **The location of large-scale soil moisture anomalies**  
2       **affects moisture transport and precipitation over**  
3       **southeastern South America**

4       **Chu-Chun Chen<sup>1</sup> and Francina Dominguez<sup>1</sup>**

5       <sup>1</sup>Department of Atmospheric Sciences, University of Illinois Urbana-Champaign, Urbana, IL 61801

6       **Key Points:**

- 7       • The impact of dry soil moisture anomalies (SMAs) on Southeastern South America  
8       (SESA) regional climate is sensitive to the location of SMAs  
9       • This study provides a causal mechanism linking soil moisture to precipitation via  
10      atmospheric circulation  
11      • When western SESA has dry soil, it generates anomalous geostrophic wind, which is  
12      co-located with the low-level jet exit region

---

Corresponding author: Francina Dominguez, [francina@illinois.edu](mailto:francina@illinois.edu)

## Abstract

Southeastern South America (SESA) is a highly productive agricultural region and a hot spot for land-atmosphere interactions. To evaluate the impact of dry soil moisture anomalies (SMAs) on SESA climate and the sensitivity of the regional climate response to the location of SMAs, we perform three experimental simulations using the Community Earth System Model (CESM) with prescribed dry SMAs over (1) SESA, (2) western SESA, and (3) eastern SESA. The dry eastern SESA simulation shows widespread negative precipitation anomalies. In contrast, the dry western SESA simulation shows positive precipitation anomalies over northeastern Argentina, which are associated with the enhanced southward moisture flux co-located with the South American low-level jet exit region. A composite analysis of extremely dry cases over western SESA using reanalysis data agrees with the findings from our CESM experiment. These findings have potential implications for subseasonal forecasting in this region.

## Plain Language Summary

Large-scale soil moisture anomalies evolve slowly and can provide an opportunity for better forecasting at time scales longer than two weeks. Therefore, it is critical to understand the causal physical mechanism and evaluate whether the regional climate response is sensitive to the location of soil moisture anomalies, especially in a productive agricultural region like southeastern South America (SESA). Using a numerical climate model, we simulate the impacts of dry soil over (1) SESA, (2) western SESA, and (3) eastern SESA. The simulations show that dry soil over Western SESA can alter regional atmospheric circulation in the proximity of the existing corridor of poleward moisture transport, hence enhancing rainfall over northeastern Argentina. Conversely, dry soil over eastern SESA or the entire SESA region results in less precipitation because enhanced northerly transport is not co-located with the low-level wind corridor. Analysis of a dataset that incorporates observations supports our findings from numerical simulations.

## 1 Introduction

Southeastern South America (SESA) is one of the most productive agricultural regions on Earth (FAO, 2016). The region is also critical for hydroelectric power and has large population centers (Barros et al., 2006). Herein, improved precipitation predictability in SESA could have far-reaching socioeconomic impacts. Land-atmosphere interactions are a promising avenue for improved predictability (Koster et al., 2011; Guo et al., 2011; Dirmeyer et al., 2018), as soil moisture anomalies (SMAs) evolve on the subseasonal to seasonal time scales. As such, understanding how SMAs affect precipitation can potentially narrow the

47 weather-climate prediction gap (Mariotti et al., 2018). SESA has been recognized as a  
48 hot spot for land-atmosphere interactions in satellite products, reanalysis data, and climate  
49 models (e.g., Ruscica et al., 2016; Spennemann et al., 2018; Baker et al., 2021). Through  
50 land-atmosphere interactions, large-scale SMAs can alter regional climate (e.g., Shukla &  
51 Mintz, 1982; Koster et al., 2014; Teng et al., 2019); one of the pathways is by changing  
52 the atmospheric circulation and associated moisture transport (Oglesby & Erickson, 1989;  
53 Grimm et al., 2007; Yang & Dominguez, 2019; Bieri et al., 2021). An important moisture  
54 source for SESA is the moisture transported from lower latitudes, which is closely related to  
55 South American low-level jet (SALLJ) activity (Nicolini et al., 2002; Marengo et al., 2004;  
56 Vera et al., 2006; Salio et al., 2007; Arraut et al., 2012). Previous studies have shown that  
57 intense rainfall events in SESA are linked to low-level jet activity (Monaghan et al., 2010).

58 The effect of the land surface on South America's overlying atmosphere has been  
59 quantified using different coupling metrics (Spennemann & Saulo, 2015; Sörensson &  
60 Menéndez, 2011; Ruscica et al., 2015). These metrics highlight regions of positive soil  
61 moisture-precipitation feedbacks over the South Atlantic Convergence Zone (Spennemann  
62 & Saulo, 2015) and eastern SESA (Sörensson & Menéndez, 2011), and negative feedbacks  
63 over western SESA (Sörensson & Menéndez, 2011). The location-dependent results from  
64 these studies imply that the precipitation response to SMAs is sensitive to the location of  
65 SMAs. However, because these coupling metrics are calculated grid point by grid point,  
66 neither the location where large-scale SMAs strongly influence regional climate nor the  
67 underlying mechanisms can be identified.

68 Previous studies have proposed mechanisms to explain how dry SMAs can affect  
69 moisture transport and precipitation. Global climate model experiments show that dry  
70 SMAs over SESA lead to anomalous cyclonic circulation and enhanced moisture transport  
71 and precipitation over SESA at monthly time scales (Bieri et al., 2021). At daily time scales,  
72 regional model simulations were used to investigate the effect of dry SMAs over northwestern  
73 Argentina (Saulo et al., 2010; Yang & Dominguez, 2019). While Yang and Dominguez  
74 (2019) have found corresponding enhanced northerly moisture transport and consequently  
75 increased precipitation, Saulo et al. (2010) did not find consistent wind anomalies in the dry  
76 northwest Argentina experiment, which may be attributed to the shorter simulation period.  
77 An analogous study, using observations of remotely sensed vegetation indices, demonstrates  
78 that increased precipitation over SESA can be linked to intensified northerly moisture flux,  
79 which is the geostrophic response to the pressure gradient induced by negative vegetation  
80 index anomalies over northern Argentina (Chug & Dominguez, 2019). Similar mechanisms  
81 have also been identified in other parts of the world, including the Great Plains of the United  
82 States (Campbell et al., 2019; Matus et al., 2023) and Africa (Talib et al., 2022, 2023).

83 However, comparison among these previous studies is challenging because of (1) the  
84 diversity in the numerical models employed and the approaches taken and (2) the lack  
85 of consistent sensitivity tests for different locations of soil moisture forcing, such as the  
86 experiments done for North America (Koster et al., 2016; Teng et al., 2019). Therefore, in  
87 this study, we performed idealized experiments using the Community Earth System Model  
88 version 1 (CESM1) (Hurrell et al., 2013) that prescribe dry SMAs within SESA, western  
89 SESA, and eastern SESA to assess the sensitivity of moisture transport and precipitation  
90 response to SMAs at different locations. In addition to the idealized experiments, we also  
91 analyze the extremely dry cases using the European Centre for Medium-Range Weather  
92 Forecast (ECMWF) Reanalysis v5 (ERA5) (Hersbach et al., 2020) monthly dataset to  
93 present observational evidence for our numerical experiments. The goal of this study is to  
94 understand the mechanisms by which dry SMAs affect moisture transport and precipitation  
95 over SESA and to assess the influence of the location of SMAs.

## 96 **2 Data and methods**

### 97 **2.1 Model experiments**

98 In this study, we use the CESM1 and follow a similar model setup as in Teng et al. (Teng  
99 et al., 2019). CESM1 consists of atmosphere, ocean, land, sea ice, and land ice components.  
100 In our simulation setup, the model has 30 vertical levels and a horizontal resolution of  
101 approximately  $1^\circ$  ( $0.9^\circ \times 1.25^\circ$ ). Since we focus on the land-atmosphere interactions, we  
102 used the “F1850LENS” component set, which activates land and atmosphere components  
103 while deactivating or prescribing other components. The sea surface temperatures and sea  
104 ice concentrations are prescribed using the monthly mean climatology averaged over years  
105 402-1510 of the fully coupled preindustrial control run of the CESM1 large ensemble project  
106 (Kay et al., 2015).

107 We performed one control simulation and three experimental simulations, each  
108 comprising 30 ensemble members initialized with varying initial conditions. The 30  
109 initial conditions are taken from the last 500 years (at least five years apart) of the  
110 atmosphere/land-only control run of the CESM1 large ensemble project. For the control  
111 simulation, each ensemble member was initialized from January and ended after running  
112 for 15 months. For the three experimental simulations, within selected domains, we  
113 prescribed the entire column of soil water to zero at each time step. As shown in Fig.  
114 1a, 2a, and S1a, the domains we selected are (1) SESA ( $67^\circ\text{W}$ - $45^\circ\text{W}$ ,  $24^\circ\text{S}$ - $40^\circ\text{S}$ ), (2)  
115 western SESA ( $67^\circ\text{W}$ - $60^\circ\text{W}$ ,  $24^\circ\text{S}$ - $40^\circ\text{S}$ ), and (3) eastern SESA ( $60^\circ\text{W}$ - $45^\circ\text{W}$ ,  $24^\circ\text{S}$ - $40^\circ\text{S}$ ).  
116 The experimental simulations started from September (using the restart files from control

117 simulations) and ended after running for 7 months, covering austral spring to early fall,  
118 because land-atmosphere interactions are stronger during summer (Koster & Suarez, 1995).

## 119 **2.2 Data**

120 To validate the simulated results, we used monthly ERA5 data spanning the period 1979  
121 to 2021. ERA5 reanalysis assimilates various sources of observations into the Integrated  
122 Forecasting System Cy41r2 model, providing a complete global estimate and a wide range  
123 of meteorological variables with 37 vertical pressure levels and a horizontal resolution of 0.25  
124 degrees. Root-zone soil moisture is calculated via a weighted average based on the soil layer  
125 thickness of the top three layers of volumetric soil water (layer 1: 0-7cm, layer 2: 7-28cm,  
126 layer 3: 28-100cm).

## 127 **2.3 Extremely dry cases selection**

128 We compare our idealized experiments with extremely dry cases from ERA5 reanalysis  
129 to verify the simulated results. First, we chose months between October and January  
130 because we focus on seasons with relatively strong land-atmosphere interactions. Second,  
131 we calculated the SMAs of each month by removing the monthly climatology averaged  
132 from 1981 to 2010. Third, we ranked the area-averaged root-zone SMAs over western  
133 SESA and selected the driest 3% months during the study period (Table S1). In these  
134 extremely dry cases, we then calculated the composite anomalies of surface heat fluxes and  
135 other atmospheric variables corresponding to the month following the dry soil moisture  
136 months. The significance of the differences between extremely dry cases and climatology  
137 was determined using the Student's  $t$ -test.

## 138 **3 Results**

### 139 **3.1 CESM simulations**

140 Fig. 1 shows the difference between the ensemble average of the dry SESA simulations  
141 and the control simulations in December; area-averaged values are shown in Table S2. The  
142 dry SMAs decrease the surface latent heat flux significantly because of the reduction of  
143 available water from the soil (Fig. 1a and b). Since the change in incoming radiation  
144 (net shortwave radiation and upwelling longwave radiation) is small (Table S2), the surface  
145 temperature and the surface sensible heat flux increase (Fig. 1c) to compensate for the  
146 decrease in surface latent heat flux, which consequently increase 2-m temperature (Fig.  
147 1d). Warming near the surface induces a thermal low and lower geopotential heights at  
148 850 hPa within SESA (Figs. 1e and f). In addition, the warming increases the thickness

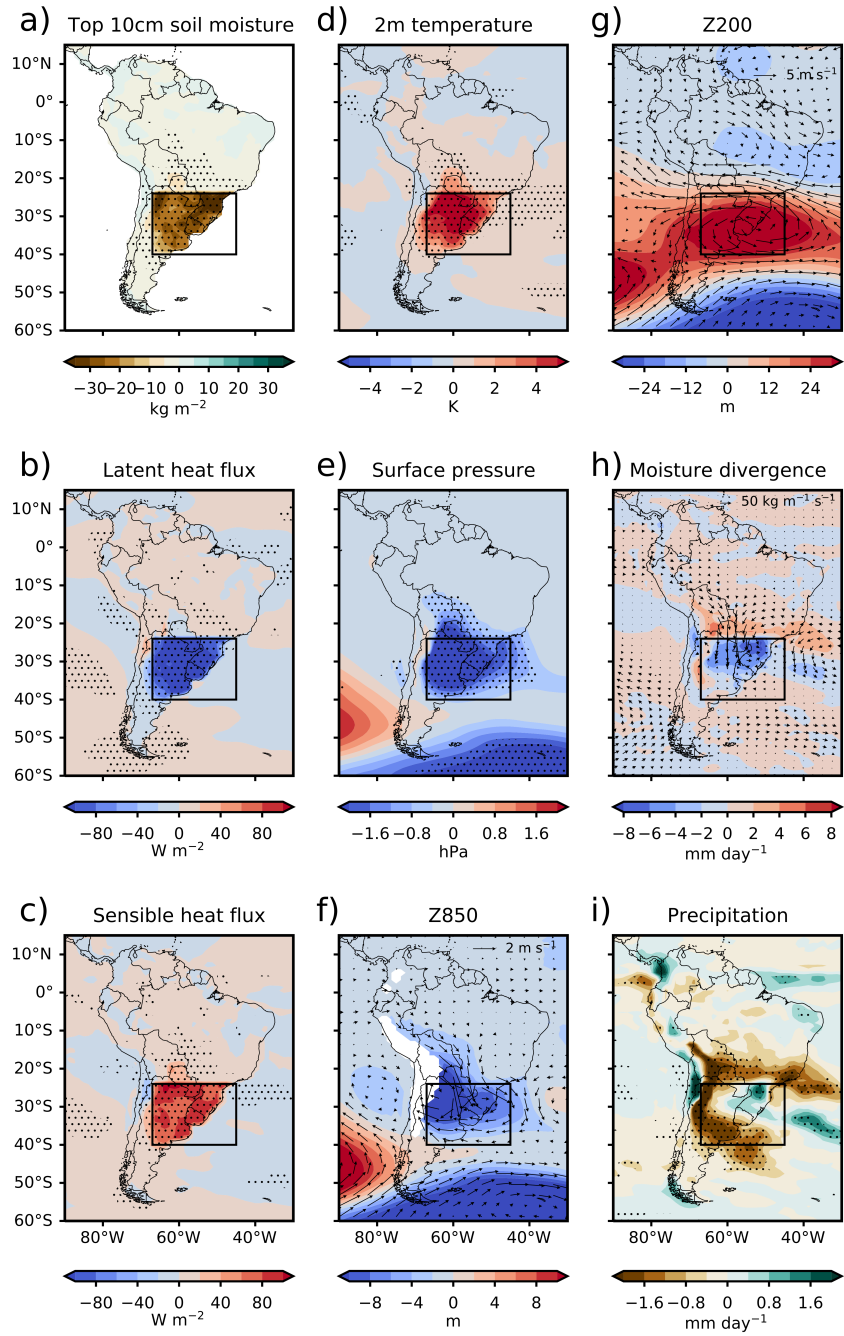


**Figure 1.** Difference between the ensemble average of the dry SESA simulations and the control simulations in December (a) soil water in top 10 cm, (b) surface latent heat flux, (c) surface sensible heat flux, (d) 2-m temperature, (e) surface pressure, (f) geopotential height and wind at 850 hPa, (g) geopotential height and wind at 200 hPa, (h) vertically integrated moisture flux divergence and moisture flux, and (i) precipitation. The box indicates the region for which the idealized soil moisture anomalies are prescribed. Stippling indicates statistically significant differences ( $p$ -value less than or equal to 0.05).

149 in the lower troposphere, leading to an increase in the geopotential heights at the upper  
150 level (Fig. 1g). The difference in vertically integrated moisture flux shows an enhanced  
151 southward moisture flux into SESA, and moisture flux converges over northern Argentina  
152 and southern Brazil (blue shading in Fig. 1h). The precipitation decreases over central  
153 and northwestern Argentina but increases over southern Brazil (Fig. 1i). The increased  
154 precipitation corresponds to the strongest moisture flux convergence.

155 We further investigate if the dry SMAs in the western and eastern parts of SESA have  
156 different impacts. Fig. 2 shows the difference between the ensemble average of the dry  
157 western SESA simulations and the control simulations in December; area-averaged values  
158 are shown in Table S3. Dry SMAs over western SESA also reduce the surface latent heat  
159 flux (Fig. 2a and b) and increase the surface sensible heat flux (Fig. 2c) within the domain.  
160 The 2-m temperature increases as well (Fig. 2d), but the magnitude is smaller than that  
161 in the dry SESA run. The surface pressure and 850 hPa geopotential height decrease  
162 mostly within the domain (Figs. 2e and f). On the other hand, geopotential height at 200  
163 hPa increases over the southern part of the domain and neighboring regions, suggesting  
164 potential nonlocal effects (Fig. 2g). The southward vertically integrated moisture flux  
165 and anomalous moisture flux convergence intensify (Fig. 2h), corresponding to increased  
166 precipitation over northeastern Argentina (Fig. 2i). The region with negative precipitation  
167 anomalies is narrower compared to the anomalies observed in the dry SESA run (Figs. 2i  
168 and 1i).

169 Fig. S1 shows the difference between the ensemble average of the dry eastern SESA  
170 simulations and the control simulations in December; area-averaged values are shown in  
171 Table S4. Similar to the responses in the dry SESA run and the dry western SESA run, the  
172 surface latent heat flux decreases because of the dry SMAs (Fig. S1a and b), and the surface  
173 sensible heat flux and 2-m temperature increase (Figs. S1c and d), although the anomalies  
174 extend slightly to the west of the eastern SESA domain. The dry eastern SESA run also  
175 has lower surface pressure and lower geopotential height at 850 hPa over the domain and  
176 the surrounding regions compared to the control run (Figs. S1e and f). There is a positive  
177 geopotential height anomaly at 200 hPa as well, with larger anomalies over the eastern part  
178 of the domain (Fig. S1g). Although there is moisture flux convergence within the domain,  
179 there is a weaker anomalous southward vertically integrated moisture flux into SESA (Fig.  
180 S1h) compared with that in the dry western SESA run (Fig. 2h). The area with negative  
181 precipitation anomalies is larger compared with the dry western SESA run, covering the  
182 central Andes, northern Argentina, and Paraguay, while only a small portion of southern  
183 Brazil shows positive precipitation anomalies (Fig. S1i).

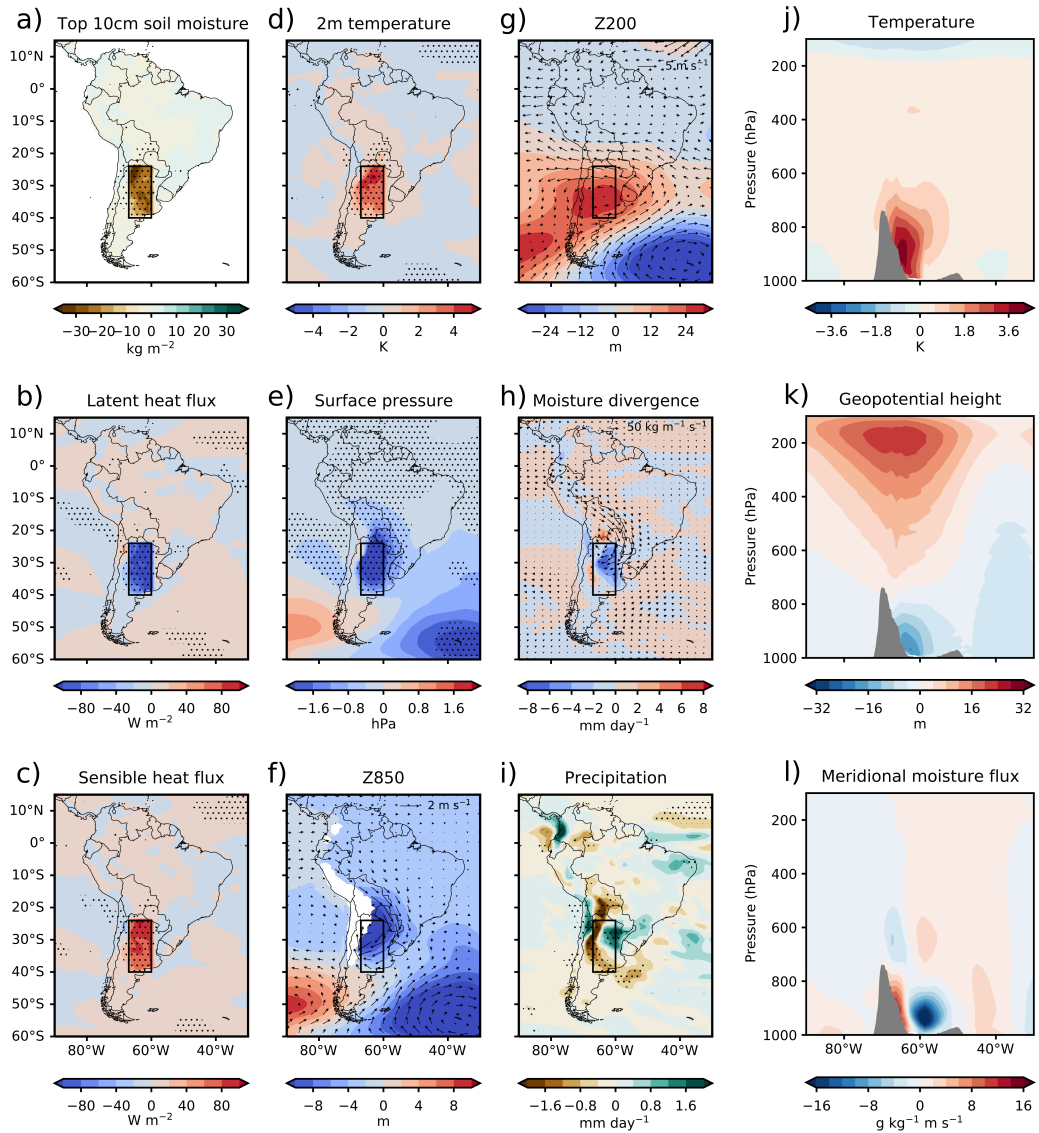


**Figure 2.** (a) to (i) as in Fig. 1, but for the dry western SESA simulations. Vertical cross sections of (j) temperature, (k) geopotential height, and (l) meridional moisture flux are anomalies between the ensemble average of the dry western SESA simulations and the control simulations in December. Gray shading indicates the topography. Values in vertical cross sections have the same longitude range as in (a) to (i) and are averaged between 24°S and 40°S.

184 We further examine pressure-longitude cross sections averaged between 24°S and 40°S.  
185 Figures 2j-l show the difference in temperature, geopotential height, and meridional moisture  
186 flux between the dry western SESA run and the control run in December. Warming at  
187 the surface and lower troposphere (Fig. 2j) decreases lower-level and increases upper-level  
188 geopotential heights (Fig. 2k) over the western SESA. The baroclinicity and the zonal  
189 gradient of the geopotential height influence the meridional moisture transport on both  
190 sides of the domain: on the eastern boundary of the domain, the positive zonal gradient of  
191 low-level geopotential height anomalies leads to enhanced low-level southward moisture flux;  
192 on the western boundary of the domain, the negative zonal gradient of low-level geopotential  
193 height anomalies weakens low-level southward moisture flux (Fig. 2l). The control run and  
194 the dry western SESA run show that the low-level southward moisture flux accelerates on  
195 the eastern boundary of the domain and decelerates on the western boundary of the domain,  
196 although the deceleration is inconspicuous because it is close to the mountain regions (Fig.  
197 S2). Critically, the enhanced low-level southward moisture flux in the dry western SESA  
198 run (Fig. 2l) is co-located with the strong southward moisture flux in the control run  
199 (Fig. S2a). Similar responses can be observed in the dry SESA run (Fig. S3) and the  
200 dry eastern SESA run (Fig. S4). However, unlike the western SESA case, the enhanced  
201 southward moisture flux in the SESA and eastern SESA runs does not correspond to the  
202 location of the southward moisture flux over land in the control run (Figs. S3c, S4c, and  
203 S2a). Additionally, in the dry eastern SESA run, the western boundary of the domain  
204 exhibits an anomalous northward flux (Fig. S4c), which then leads to the widespread  
205 negative precipitation anomalies (Fig. S1i). The distinct responses among experimental  
206 runs highlight the sensitivity of precipitation and moisture transport to the location of  
207 SMAs over SESA.

### 208 3.2 ERA5 reanalysis

209 Fig. 3 shows the difference between the extremely dry cases and climatology;  
210 area-averaged values are shown in Table S5. Antecedent SMAs over western SESA (Fig.  
211 3a) are associated with decreased surface latent heat flux (Fig. 3b) and increased surface  
212 sensible heat flux (Fig. 3c) within the same domain. The 2-m temperature increases over  
213 northern Argentina and neighboring areas (Fig. 3d), which is similar to the response in  
214 the dry western SESA CESM1 simulation (Fig. 2d). There are negative surface pressure  
215 anomalies and lower geopotential height anomalies at 850 hPa mostly over the western SESA  
216 (Figs. 3e and f), while the geopotential height at 200 hPa increases over the entire SESA  
217 (Fig. 3g). The anomalous moisture convergence over northeastern Argentina and Paraguay  
218 (Fig. 3h) corresponds to increased precipitation over the same region (Fig. 3i).

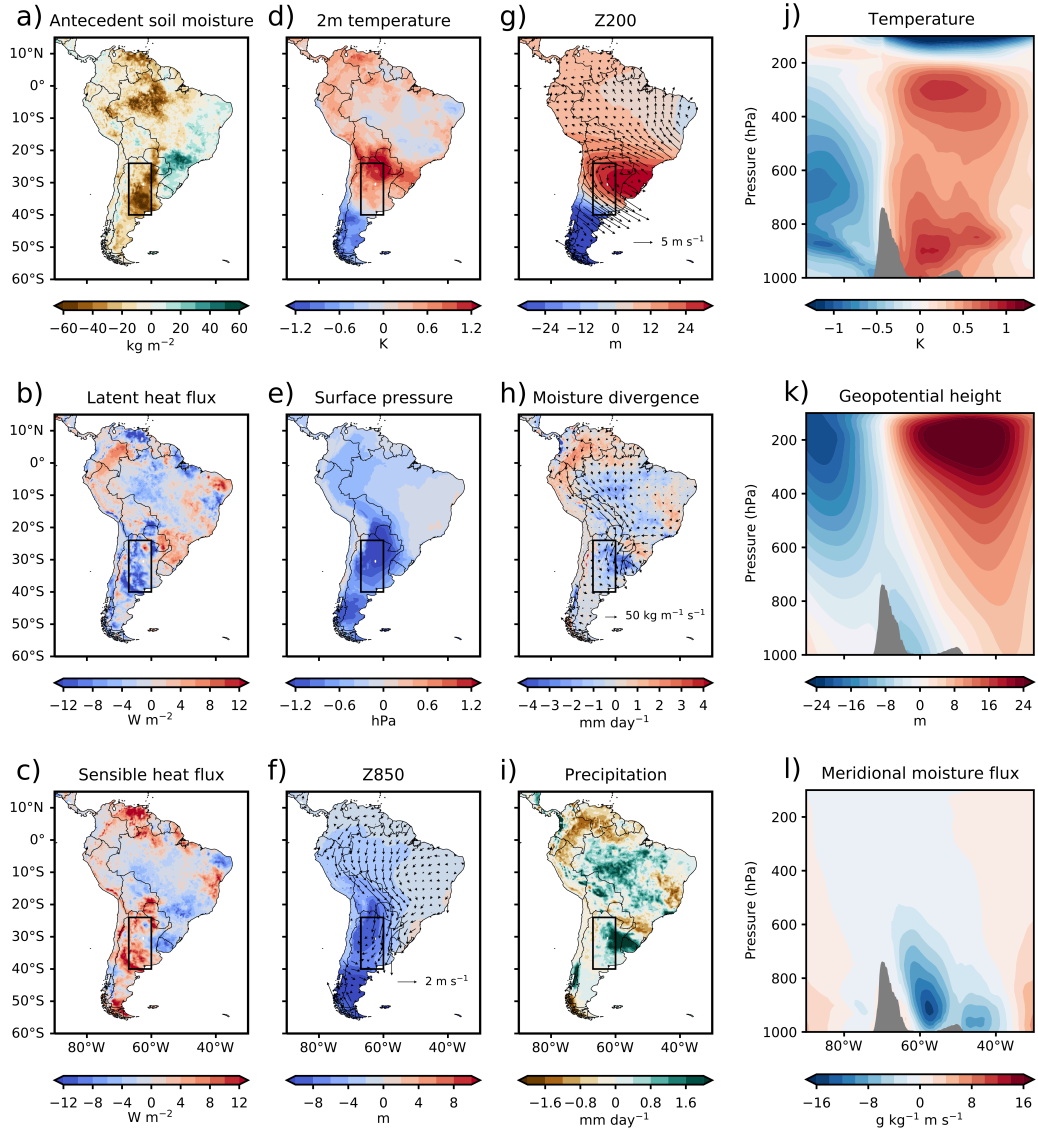


**Figure 3.** (b) to (l) as in Fig. 2, but for the difference between the ERA5 reanalysis extremely dry western SESA cases and climatology. (a) is the difference in antecedent soil moisture in top 1 m.

219 Fig. 3j-l shows pressure-longitude cross sections of temperature, geopotential height,  
220 and meridional moisture flux anomalies averaged between 24°S and 40°S in the extremely  
221 dry western SESA cases compared to climatology. There is warming at both the lower  
222 troposphere and the upper troposphere (Fig. 3j), and the low-level warming corresponds to  
223 decreased low-level geopotential height over western SESA (Fig. 3k). On the east side of  
224 the domain, the positive zonal gradient of low-level geopotential height also corresponds to  
225 intensified southward moisture flux, although there is no apparent deceleration on the west  
226 side of the domain (Fig. 3l).

227 Overall, the responses in ERA5 reanalysis and in CESM simulations are quite similar.  
228 Slight differences between the extremely dry cases and the idealized experimental runs are  
229 reasonable because the responses in the extremely dry cases are a combination of signals  
230 from SMAs and other forcings.

## 231 4 Discussion

232 The results from our CESM simulations and ERA5 reanalysis suggest that dry  
233 SMAs can lead to lower troposphere warming and geopotential height anomalies, causing  
234 anomalous geostrophic flows, which can influence moisture fluxes and precipitation over  
235 SESA. This is consistent with previous studies that show that the thermal low induced by  
236 dry SMAs affects local circulation and further influences precipitation (Grimm et al., 2007;  
237 Chug & Dominguez, 2019; Yang & Dominguez, 2019; Bieri et al., 2021). It is also supported  
238 by previous studies that these circulation changes could be linked to the northwestern  
239 Argentinean low and the SALLJ (Chug & Dominguez, 2019; Yang & Dominguez, 2019).  
240 Note that Chug and Dominguez (2019) focus on observed vegetation index anomalies instead  
241 of SMAs, but the browning (negative) vegetation index anomalies are located over western  
242 SESA and have similar surface forcings (surface latent heat flux, surface sensible heat flux,  
243 and surface temperature) and atmospheric responses (thermal low, southerly wind, and  
244 precipitation) as the results shown in the western SESA experiment.

245 One of the implications of this work is that the relation between soil moisture and  
246 precipitation can affect the length and intensity of droughts, which is also discussed in Bieri  
247 et al. (2021). In this study, we suggest that this relation is sensitive to the location of  
248 dry SMAs, and we clearly identify the physical mechanisms at play. The dry SMAs over  
249 the entire SESA or over the eastern SESA mostly induce a positive feedback between soil  
250 moisture and precipitation (i.e., dry soil leads to less precipitation, then less precipitation  
251 leads to drier soil), which has been the focus of most previous studies (e.g., Shukla & Mintz,  
252 1982; Findell & Eltahir, 1997; Eltahir, 1998; Seneviratne et al., 2010). This positive feedback  
253 may result in a longer or stronger drought. On the contrary, the dry SMAs over the western

254 SESA induce a negative feedback between soil moisture and precipitation over most of the  
255 region, indicating that the dry soil is associated with positive precipitation anomalies, which  
256 would mitigate the dry SMAs. This negative feedback may lead to a shorter and weaker  
257 drought. Note that the precipitation responses are not exactly over the dry SMAs domain,  
258 so in addition to the changes in length and intensity, the drought may also migrate with  
259 time.

260 There are some limitations in this study related to the simulation setup. First, our  
261 idealized experiments prescribe extremely dry SMAs. Teng et al. (2019) have performed  
262 a sensitivity test of different strengths of soil moisture forcing over the Great Plains and  
263 found that there are clear and robust upper-level geopotential responses in the extremely  
264 dry simulations, while it is harder to detect signals if the soil moisture forcing is closer  
265 to the range of natural soil moisture variability in the model. Having extremely dry soil  
266 moisture forcing allows us to more clearly identify the physical mechanisms. Although we  
267 have found clear and consistent responses between the idealized CESM experiments and the  
268 extremely dry cases in ERA5 reanalysis data, further studies are warranted to examine if the  
269 mechanism found here is sensitive to the strength of SMAs. Second, we only conduct these  
270 experiments using one model. While the representation of land-atmosphere interactions  
271 may vary among different models, further research is needed to assess the potential model  
272 dependency of atmospheric response to dry SMAs. Third, the spatial resolution of the model  
273 is relatively coarse (approximately  $1^\circ$ ), so neither the topography nor mesoscale processes  
274 can be resolved in the current simulations.

275 Given that the purpose of this study is to bridge the subseasonal to seasonal prediction  
276 gap, we are focusing on monthly time scales. The results here should be interpreted as a  
277 long-term mean of atmospheric responses to dry soil moisture at a large spatial scale instead  
278 of direct impacts of dry SMAs on SALLJ.

## 279 **5 Conclusions**

280 In this study, three idealized prescribed soil moisture experiments were performed and  
281 compared with a control simulation using CESM. The soil moisture within SESA, western  
282 SESA, and eastern SESA is prescribed to zero in the experimental simulations to assess the  
283 impact of dry SMAs at different locations on the regional climate. Our results show that  
284 these experimental runs exhibit distinct precipitation responses associated with anomalous  
285 meridional moisture flux. We validated the model simulations by analyzing extremely dry  
286 cases over western SESA using ERA5 reanalysis and found similar responses as in the  
287 western SESA simulations.

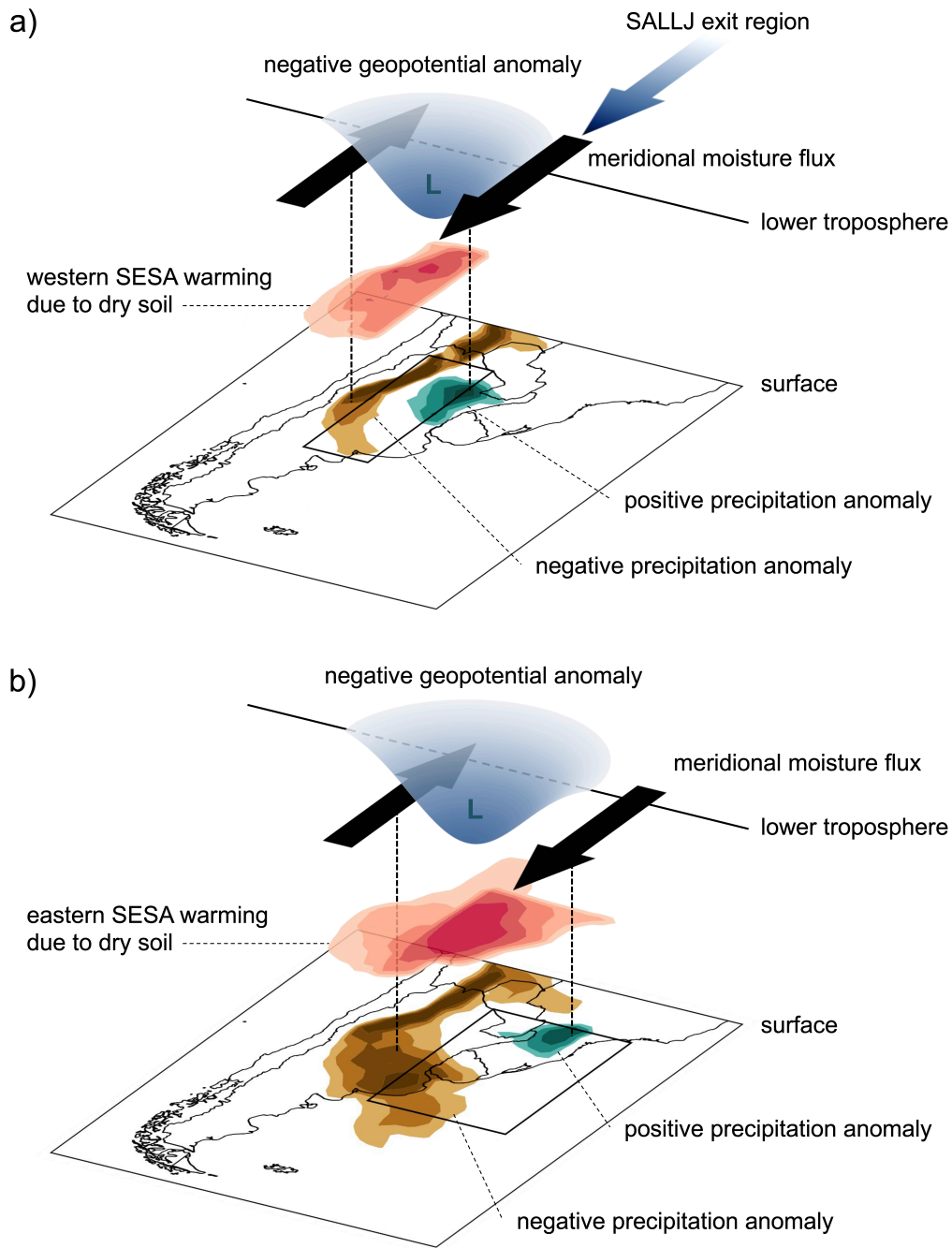


**Figure 4.** Schematic of the different regional climate responses corresponding to dry soil moisture anomalies over (a) western SESA and (b) eastern SESA. Red shading indicates the anomalous warming at the surface and lower troposphere. Blue shading with the letter L indicates the negative geopotential height anomalies associated with the warming and thermal low at the lower troposphere. Black arrows indicate meridional moisture flux anomalies associated with the geostrophic responses. Green and brown shadings indicate positive and negative precipitation anomalies, respectively. Blue arrow in (a) indicates the SALLJ exit region.

288 Fig. 4 summarizes the proposed physical mechanism and highlights the distinct climate  
289 responses to dry SMAs over western and eastern SESA. On the one hand, when dry SMAs  
290 extend over western SESA, the surface warming results in a geostrophic wind anomaly, which  
291 is co-located with the SALLJ exit region, enhancing the southward meridional moisture  
292 flux and increasing precipitation over northeastern Argentina; near the western boundary  
293 of western SESA, the area of anomalous meridional moisture flux is narrower, since it is  
294 near the mountain regions and is affected by topography (Fig. 4a). On the other hand,  
295 when dry SMAs extend over eastern SESA, the surface warming also leads to changes in  
296 geopotential height anomalies, resulting in anomalous southward meridional moisture fluxes  
297 on the eastern boundary of the domain and increased precipitation over a small portion of  
298 southern Brazil and over the ocean, but the magnitude is smaller because enhanced moisture  
299 flux is not co-located with the SALLJ exit region; near the western boundary of the domain,  
300 the geopotential height anomalies induce northward meridional fluxes, which are associated  
301 with a large area of negative precipitation anomalies (Fig. 4b).

302 This study provides a causal mechanism of the effect of large-scale SMAs over SESA on  
303 precipitation and moisture transport, complementing previous studies. Furthermore, this  
304 is the first study to assess the sensitivity of monthly climate response to large-scale SMAs  
305 at different locations over SESA. The dry SMAs in western SESA correspond to a negative  
306 feedback between soil moisture and precipitation, while the dry SMAs in eastern SESA  
307 correspond to a positive feedback. These different relationships between soil moisture and  
308 precipitation imply that the location of the dry SMAs may affect the length and intensity of  
309 droughts, which have potential implications for subseasonal drought forecasting over SESA.

## 310 **Open Research**

311 The CESM1 (Hurrell et al., 2013) model code is available at [https://www2.cesm.ucar.edu/  
312 models/cesm1.1/](https://www2.cesm.ucar.edu/models/cesm1.1/). The ERA5 data (Hersbach et al., 2020) are available at [https://  
313 doi.org/10.24381/cds.f17050d7](https://doi.org/10.24381/cds.f17050d7) (variables on single levels) and at [https://doi.org/  
314 10.24381/cds.6860a573](https://doi.org/10.24381/cds.6860a573) (variables on pressure levels). The data and the code used  
315 to analyze the results in this study are archived in the University of Illinois' Data  
316 Bank (temporary link: [https://databank.illinois.edu/datasets/IDB-0536017?code=  
317 P22ca7oGTZNudm-CmKwMhNWGtsTQP17wY5w\\_X5PUJoQ](https://databank.illinois.edu/datasets/IDB-0536017?code=P22ca7oGTZNudm-CmKwMhNWGtsTQP17wY5w_X5PUJoQ), we will replace this temporary link  
318 with a permanent DOI upon publication).

## 319 **Acknowledgments**

320 This work was supported by the National Science Foundation (NSF) award 1852709.  
321 We would like to acknowledge high-performance computing support from Cheyenne

322 (doi:10.5065/D6RX99HX) provided by NCAR's Computational and Information Systems  
323 Laboratory, sponsored by the NSF. We thank Dr. Haiyan Teng for providing guidance on  
324 setting up the CESM experiments and offering valuable advice.

## 325 References

- 326 Arraut, J. M., Nobre, C., Barbosa, H. M. J., Obregon, G., & Marengo, J. (2012).  
327 Aerial rivers and lakes: Looking at large-scale moisture transport and its relation  
328 to Amazonia and to subtropical rainfall in South America. *Journal of Climate*, *25*(2),  
329 543–556. doi: 10.1175/2011JCLI4189.1
- 330 Baker, J. C. A., Souza, D. C. d., Kubota, P. Y., Buermann, W., Coelho, C. A. S., Andrews,  
331 M. B., ... Spracklen, D. V. (2021). An assessment of land–atmosphere interactions  
332 over South America using satellites, reanalysis, and two global climate models. *Journal*  
333 *of Hydrometeorology*, *22*(4), 905–922. doi: 10.1175/JHM-D-20-0132.1
- 334 Barros, V., Clarke, R., & Silva Días, P. (2006). *Climate change in the La Plata basin*.  
335 Retrieved 2023-06-12, from [https://www2.atmos.umd.edu/~berbery/lpb/climate](https://www2.atmos.umd.edu/~berbery/lpb/climate_change_lpb.pdf)  
336 [\\_change\\_lpb.pdf](https://www2.atmos.umd.edu/~berbery/lpb/climate_change_lpb.pdf)
- 337 Bieri, C. A., Dominguez, F., & Lawrence, D. M. (2021). Impacts of large-scale soil  
338 moisture anomalies on the hydroclimate of southeastern South America. *Journal of*  
339 *Hydrometeorology*, *22*(3), 657–669. doi: 10.1175/JHM-D-20-0116.1
- 340 Campbell, M. A., Ferguson, C. R., Burrows, D. A., Beauharnois, M., Xia, G., & Bosart, L. F.  
341 (2019). Diurnal effects of regional soil moisture anomalies on the Great Plains low-level  
342 jet. *Monthly Weather Review*, *147*(12), 4611–4631. doi: 10.1175/MWR-D-19-0135.1
- 343 Chug, D., & Dominguez, F. (2019). Isolating the observed influence of vegetation variability  
344 on the climate of La Plata River basin. *Journal of Climate*, *32*(14), 4473–4490. doi:  
345 10.1175/JCLI-D-18-0677.1
- 346 Dirmeyer, P. A., Halder, S., & Bombardi, R. (2018). On the harvest of predictability from  
347 land states in a global forecast model. *Journal of Geophysical Research: Atmospheres*,  
348 *123*(23), 13,111–13,127. doi: 10.1029/2018JD029103
- 349 Eltahir, E. A. B. (1998). A soil moisture–rainfall feedback mechanism: 1. Theory and  
350 observations. *Water Resources Research*, *34*(4), 765–776. doi: 10.1029/97WR03499
- 351 FAO. (2016). *AQUASTAT transboundary river basin overview – La Plata*. Food and  
352 *Agriculture Organization of the United Nations (FAO)*. Rome, Italy. Retrieved  
353 2023-06-08, from <https://www.fao.org/publications/card/en/c/CA2141EN/>
- 354 Findell, K. L., & Eltahir, E. A. B. (1997). An analysis of the soil moisture–rainfall feedback,  
355 based on direct observations from Illinois. *Water Resources Research*, *33*(4), 725–735.  
356 doi: 10.1029/96WR03756
- 357 Grimm, A. M., Pal, J. S., & Giorgi, F. (2007). Connection between spring conditions

- 358 and peak summer monsoon rainfall in South America: Role of soil moisture,  
359 surface temperature, and topography in eastern Brazil. *Journal of Climate*, *20*(24),  
360 5929–5945. doi: 10.1175/2007JCLI1684.1
- 361 Guo, Z., Dirmeyer, P. A., & DelSole, T. (2011). Land surface impacts on subseasonal  
362 and seasonal predictability. *Geophysical Research Letters*, *38*(24). doi: 10.1029/  
363 2011GL049945
- 364 Hersbach, H., Bell, B., Berrisford, P., Hirahara, S., Horányi, A., Muñoz-Sabater, J., ...  
365 Thépaut, J.-N. (2020). The ERA5 global reanalysis. *Quarterly Journal of the Royal*  
366 *Meteorological Society*, *146*(730), 1999–2049. doi: 10.1002/qj.3803
- 367 Hurrell, J. W., Holland, M. M., Gent, P. R., Ghan, S., Kay, J. E., Kushner, P. J.,  
368 ... Marshall, S. (2013). The Community Earth System Model: A framework  
369 for collaborative research. *Bulletin of the American Meteorological Society*, *94*(9),  
370 1339–1360. doi: 10.1175/BAMS-D-12-00121.1
- 371 Kay, J. E., Deser, C., Phillips, A., Mai, A., Hannay, C., Strand, G., ... Vertenstein, M.  
372 (2015). The Community Earth System Model (CESM) Large Ensemble project: A  
373 community resource for studying climate change in the presence of internal climate  
374 variability. *Bulletin of the American Meteorological Society*, *96*(8), 1333–1349. doi:  
375 10.1175/BAMS-D-13-00255.1
- 376 Koster, R. D., Chang, Y., & Schubert, S. D. (2014). A mechanism for land–atmosphere  
377 feedback involving planetary wave structures. *Journal of Climate*, *27*(24), 9290–9301.  
378 doi: 10.1175/JCLI-D-14-00315.1
- 379 Koster, R. D., Chang, Y., Wang, H., & Schubert, S. D. (2016). Impacts of local soil moisture  
380 anomalies on the atmospheric circulation and on remote surface meteorological fields  
381 during boreal summer: A comprehensive analysis over North America. *Journal of*  
382 *Climate*, *29*(20), 7345–7364. doi: 10.1175/JCLI-D-16-0192.1
- 383 Koster, R. D., Mahanama, S. P. P., Yamada, T. J., Balsamo, G., Berg, A. A., Boisserie, M.,  
384 ... Wood, E. F. (2011). The second phase of the Global Land–Atmosphere Coupling  
385 Experiment: Soil moisture contributions to subseasonal forecast skill. *Journal of*  
386 *Hydrometeorology*, *12*(5), 805–822. doi: 10.1175/2011JHM1365.1
- 387 Koster, R. D., & Suarez, M. J. (1995). Relative contributions of land and ocean processes  
388 to precipitation variability. *Journal of Geophysical Research: Atmospheres*, *100*(D7),  
389 13775–13790. doi: 10.1029/95JD00176
- 390 Marengo, J. A., Soares, W. R., Saulo, C., & Nicolini, M. (2004). Climatology of the low-level  
391 jet east of the Andes as derived from the NCEP–NCAR reanalyses: Characteristics  
392 and temporal variability. *Journal of Climate*, *17*(12), 2261–2280. doi: 10.1175/1520-  
393 -0442(2004)017(2261:COTLJE)2.0.CO;2
- 394 Mariotti, A., Ruti, P. M., & Rixen, M. (2018). Progress in subseasonal to seasonal prediction

- 395 through a joint weather and climate community effort. *npj Climate and Atmospheric*  
396 *Science*, 1(1), 1–4. doi: 10.1038/s41612-018-0014-z
- 397 Matus, S. A., Dominguez, F., & Ford, T. W. (2023). Land and atmosphere conditions prior  
398 to extreme Great Plains low-level jets. *Journal of Hydrometeorology*, 24(4), 783–800.  
399 doi: 10.1175/JHM-D-22-0045.1
- 400 Monaghan, A. J., Rife, D. L., Pinto, J. O., Davis, C. A., & Hannan, J. R. (2010). Global  
401 precipitation extremes associated with diurnally varying low-level jets. *Journal of*  
402 *Climate*, 23(19), 5065–5084. doi: 10.1175/2010JCLI3515.1
- 403 Nicolini, M., Saulo, A. C., Torres, J. C., & Salio, P. (2002). Enhanced precipitation over  
404 southeastern South America related to strong low-level jet events during austral warm  
405 season. *Meteorologica*, 27, 59–70.
- 406 Oglesby, R. J., & Erickson, D. J. (1989). Soil moisture and the persistence of North American  
407 drought. *Journal of Climate*, 2(11), 1362–1380. doi: 10.1175/1520-0442(1989)  
408 002<1362:SMATPO>2.0.CO;2
- 409 Ruscica, R. C., Menéndez, C. G., & Sörensson, A. A. (2016). Land surface–atmosphere  
410 interaction in future South American climate using a multi-model ensemble.  
411 *Atmospheric Science Letters*, 17(2), 141–147. doi: 10.1002/asl.635
- 412 Ruscica, R. C., Sörensson, A. A., & Menéndez, C. G. (2015). Pathways between soil moisture  
413 and precipitation in southeastern South America. *Atmospheric Science Letters*, 16(3),  
414 267–272. doi: 10.1002/asl2.552
- 415 Salio, P., Nicolini, M., & Zipser, E. J. (2007). Mesoscale convective systems over southeastern  
416 South America and their relationship with the South American low-level jet. *Monthly*  
417 *Weather Review*, 135(4), 1290–1309. doi: 10.1175/MWR3305.1
- 418 Saulo, C., Ferreira, L., Nogués-Paegle, J., Seluchi, M., & Ruiz, J. (2010). Land–atmosphere  
419 interactions during a northwestern Argentina low event. *Monthly Weather Review*,  
420 138(7), 2481–2498. doi: 10.1175/2010MWR3227.1
- 421 Seneviratne, S. I., Corti, T., Davin, E. L., Hirschi, M., Jaeger, E. B., Lehner, I., . . . Teuling,  
422 A. J. (2010). Investigating soil moisture–climate interactions in a changing climate: A  
423 review. *Earth-Science Reviews*, 99(3), 125–161. doi: 10.1016/j.earscirev.2010.02.004
- 424 Shukla, J., & Mintz, Y. (1982). Influence of land-surface evapotranspiration on the Earth’s  
425 climate. *Science*, 215(4539), 1498–1501. doi: 10.1126/science.215.4539.1498
- 426 Spennemann, P. C., Salvia, M., Ruscica, R. C., Sörensson, A. A., Grings, F., &  
427 Karszenbaum, H. (2018). Land-atmosphere interaction patterns in southeastern South  
428 America using satellite products and climate models. *International Journal of Applied*  
429 *Earth Observation and Geoinformation*, 64, 96–103. doi: 10.1016/j.jag.2017.08.016
- 430 Spennemann, P. C., & Saulo, A. C. (2015). An estimation of the land-atmosphere  
431 coupling strength in South America using the Global Land Data Assimilation System.

- 432 *International Journal of Climatology*, 35(14), 4151–4166. doi: 10.1002/joc.4274
- 433 Sörensson, A. A., & Menéndez, C. G. (2011). Summer soil–precipitation coupling in South  
434 America. *Tellus A*, 63(1), 56–68. doi: 10.1111/j.1600-0870.2010.00468.x
- 435 Talib, J., Taylor, C. M., Harris, B. L., & Wainwright, C. M. (2023). Surface-driven  
436 amplification of Madden–Julian oscillation circulation anomalies across East Africa  
437 and its influence on the Turkana jet. *Quarterly Journal of the Royal Meteorological  
438 Society*, 149(754), 1890–1912. doi: 10.1002/qj.4487
- 439 Talib, J., Taylor, C. M., Klein, C., Harris, B. L., Anderson, S. R., & Semeena, V. S.  
440 (2022). The sensitivity of the West African monsoon circulation to intraseasonal soil  
441 moisture feedbacks. *Quarterly Journal of the Royal Meteorological Society*, 148(745),  
442 1709–1730. doi: 10.1002/qj.4274
- 443 Teng, H., Branstator, G., Tawfik, A. B., & Callaghan, P. (2019). Circumglobal response to  
444 prescribed soil moisture over North America. *Journal of Climate*, 32(14), 4525–4545.  
445 doi: 10.1175/JCLI-D-18-0823.1
- 446 Vera, C., Baez, J., Douglas, M., Emmanuel, C. B., Marengo, J., Meitin, J., ... Zipser, E.  
447 (2006). The South American Low-Level Jet Experiment. *Bulletin of the American  
448 Meteorological Society*, 87(1), 63–78. doi: 10.1175/BAMS-87-1-63
- 449 Yang, Z., & Dominguez, F. (2019). Investigating land surface effects on the moisture  
450 transport over South America with a moisture tagging model. *Journal of Climate*,  
451 32(19), 6627–6644. doi: 10.1175/JCLI-D-18-0700.1